Enhancing 3D Clay Printing with Computer Vision and Deep Learning

Aut, Serdar; Ding, X.; Guha, S.; Ryu, S.; Wei, W.

Publication date
2025

Document Version
Final published version

Published in
eCAADe 43

Enhancing 3D Clay Printing with Computer Vision and Deep Learning

Serdar Aşut[1], Xiaochen Ding[2], Swornava Guha[3], Sanguk Ryu[4], Wei Wei[5]
[1,2,3,4,5]Delft University of Technology, Faculty of Architecture and the Built Environment
[1]s.asut@tudelft.nl [2]xdin952@outlook.com [3]swornava.guha@gmail.com
[4]sanguk.ryu94@gmail.com [5]weiwei3748@gmail.com

This paper presents an ongoing project that explores the usability of computer vision and deep learning to improve the quality of 3D clay printing (3DCP). One of the challenges in 3DCP is related to the nonstandard nature of the clay mixture and the environmental conditions in which the printing happens, which can result in printing failures. Manual interventions are required to adjust the printing parameters to ensure a good result. In this project, we aimed to develop an automated solution to this challenge by using computer vision and the Attention-56 deep learning network (DLN) method presented by Wang et al. (2017) and the real-time material flow control method presented by Brion and Pattinson (2022a, 2022b). Our work adapts these methods for 3DCP to adjust layer height and extrusion amount to automatically respond to changing clay mixture properties and achieve better results.

Keywords: *3D Printing, Additive Manufacturing, Clay, Quality Monitoring, Machine Learning, Computer Vision.*

INTRODUCTION

This paper presents an ongoing project that explores the usability of computer vision and deep learning to improve the quality of 3D printing (3DP) with earth-based materials. Due to its low environmental impact, earth construction has received much consideration in recent years, including its usability assessment in 3DP (Perrot, Rangeard and Courteille 2018). The synergy between 3DP and using soils as construction materials presents extensive application opportunities, ranging from small-scale elements to large-scale structures (Asaf et al., 2023). However, 3DP with earth-based materials is a largely uncharacterized fabrication approach, which requires established methods to process earthen materials (Curth et al., 2024).

Clay, a sub-ingredient of soil that can be used as found in nature or manufactured, has received most of the attention in 3DP applications for many years compared to other earth-based mixtures, mainly due to the rheological qualities of the wet clay mixture which enhances the controllability of the 3DP process (Gomaa et al., 2022).

Recent explorations on 3D Clay Printing (3DCP) in architectural applications include advancing traditional cob construction methods through printing with clay-based mixtures (Gomaa et al., 2021, Alqenaee, Memari and Hojati, 2021), using robotic clay printing to produce modular wall component systems (Gündüz and Özkar, 2024), utilizing local clay for printed terracotta components

(El Aabbas et al., 2024), design and printing of earthen wall components that integrate ventilation systems (Taher, Aşut and van der Spoel, 2023), and printing decorative architectural elements with clay (Chan et al., 2020).

One of the challenges in 3DPC is related to the nonstandard nature of the clay mixture and the environmental conditions in which the printing happens, which can result in printing failures. Therefore, manual interventions are required to adjust the printing parameters to ensure a good result. In this project, we aimed to develop an automated solution to this challenge using computer vision and deep learning. Our work builds upon the real-time closed-loop control system presented by Brion and Pattinson (2022a, 2022b), who showed how the system can learn optimal printing parameters by training regression models for extruding thermoplastics.

There is growing research on using Machine Learning (ML) and computer vision for quality control and improvement in 3DP. The review articles of Geng et al. (2023) and Farrokhsiar, Gursoy and Duarte, (2024) present the applications relevant to architecture. Other relevant work includes a vision-based real-time extrusion quality monitoring system developed for robotic construction (Kazemian et al., 2019), an automated layer defect detection system using a deep convolutional neural network (Davtalab et al., 2020), an in-situ quality assessment and improvement technique using point clouds via laser scanning (Akhavan, Lyu and Manoochehri, 2024), a defect detection technology using the YOLOv8 algorithm to train a defect detection model capable of identifying and evaluating defect images (Wang et al., 2024), warpage detection in polymer-based parts using convolutional neural networks (Bhandarkar, Kumar and Tandon, 2025), a framework using a Data-efficient Image Transformer model to identify and classify warping, layer delamination, and gaps in raster lines in fabricating polymeric prototypes (Singh et al., 2025). More research is needed to address the use of earth-based materials to advance 3DCP.

MATERIALS AND METHODS

In this project, we transformed a standard 3DCP setup by integrating computer vision to monitor the printing process of specimens printed using different parameters. We collected images during the process and then used them to train a machine learning model based on the Attention-56 deep learning network method (Wang et al., 2017), similar to the process presented by Brion and Pattinson (2022a, 2022b). Then, the model is used to predict the ideal printing parameters, which are then used to update the G-code for final prototyping.

The standard 3DCP setup

The clay we used in this project is the PRAI 3D white stoneware adapted for 3DCP. It comes as a mixture containing 22% water, according to the manufacturer's instructions. (Keramikos, n.d.). We added 100 grams of water to a 5-kilogram clay mixture to enhance its extrudability before filling it into the printer tank.

We used a WASP 40100 printer equipped with a Liquid Deposition Modelling (LDM) extruder 3.0 with a 3 mm nozzle. The clay was filled inside a 5 L tank and extruded with 0.4 MPa air pressure. Termite 1.1 software, which is a modular slicing tool for Grasshopper designed for LDM 3D printers (Jauk, 2025), was used for slicing, adjusting the printing parameters, and generating the G-code.

Computer vision system

The computer vision system consists of a Raspberry Camera Module 3 controlled by a Raspberry Pi 4 (Model B, with 4GB RAM). It was mounted next to the extruder, targeting the nozzle. It aimed to record images at a specific interval and record them with the relevant G-code instance data.

For remote control and monitoring the printer during data collection, we used the OctoPrint for WASP software, a customized version of OctoPrint,

an open-source 3D printer management software (OctoPrint, n.d.) tailored for WASP printers. It allows remote control and monitoring of WASP printers via a web interface. The printer, Raspberry Pi, and a computer were connected through a router on a local network.

A Python script that runs on the Raspberry Pi was developed to automate the data collection process. It records the current-running G-code from the WASP printer via OctoPrint and captures time-lapse images using the Raspberry Pi camera module. The data is saved on the computer as a CSV file.

Printing the specimens

A series of specimens were printed using different layer heights and extrusion amounts to observe the correlation between these two printing parameters and the result. We aimed for the specimen to have complex geometrical features to help assess various characteristics. The design developed by Keep (2020) was utilized for this purpose as it allows the assessment of diverse geometrical features such as straight and curved edges, overhangs, and freeform patterns (Figure 1). It was printed within an 80*80*80 mm bounding volume as a single-shell print without a base and cap. Eventually, 24 specimens were printed with different layer height and extrusion amount combinations.

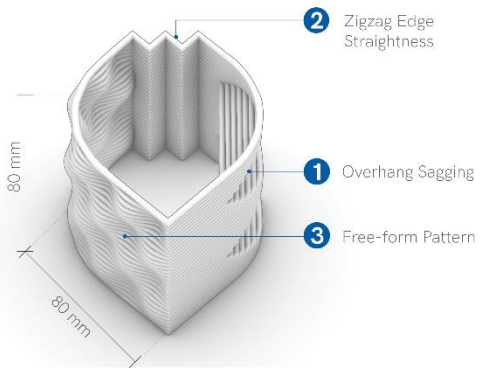

Figure 1
The design of the specimen

Rating the specimen qualities

The printed specimens were photographed under consistent artificial lighting in a closed studio using a Nikon Z50 camera with a 210 mm lens. The photographs were analyzed to assess the specimens' quality based on three geometric features: overhangs, edge straightness, and freeform patterns. Each feature was rated on a scale from 1 (poor) to 5 (excellent) .

Overhang sagging was the most noticeable sign of displacement among the three geometric characteristics. The specimens on which the overhangs were completely collapsed were scored with 1. The ones that partially collapsed or performed a so-called bridging phenomenon scored 2. Three features were measured for the specimens that performed intact: deviation area, deflection angle, and surface quality.

Figure 2-A shows the measurement method for rating the deviation area on overhangs. Using the Canny Edge Detection (CED) in Python, the extracted contour was masked and compared with the designed overhang. An additional script was then used to measure the deviated area.

Figure 2-B shows the method for measuring the deflection angle on overhangs. CED was performed starting from the corner where sagging initiates. The total value of four measured angles (top, bottom, left, and right) was recorded for assessment.

In many specimens, the overhang surface, which is supposed to be flat, displayed a wobbly pattern regardless of the deviation area or deflection angle. Thus, a qualitative assessment was conducted in addition to the earlier numerical analyses. The wobbly, moderate, or smooth surfaces were scored from 3 to 5 (Figure 2-C).

The two zigzag edge valleys were analyzed using CED (Figure 2-D). The area of the vertical line was evaluated by comparing it to a reference, masking any deviations, and quantifying displacement by area calculation. A coefficient was applied to the distance that should have been printed based on measurements taken up to the point where printing

remained intact to account for results that collapsed mid-print.

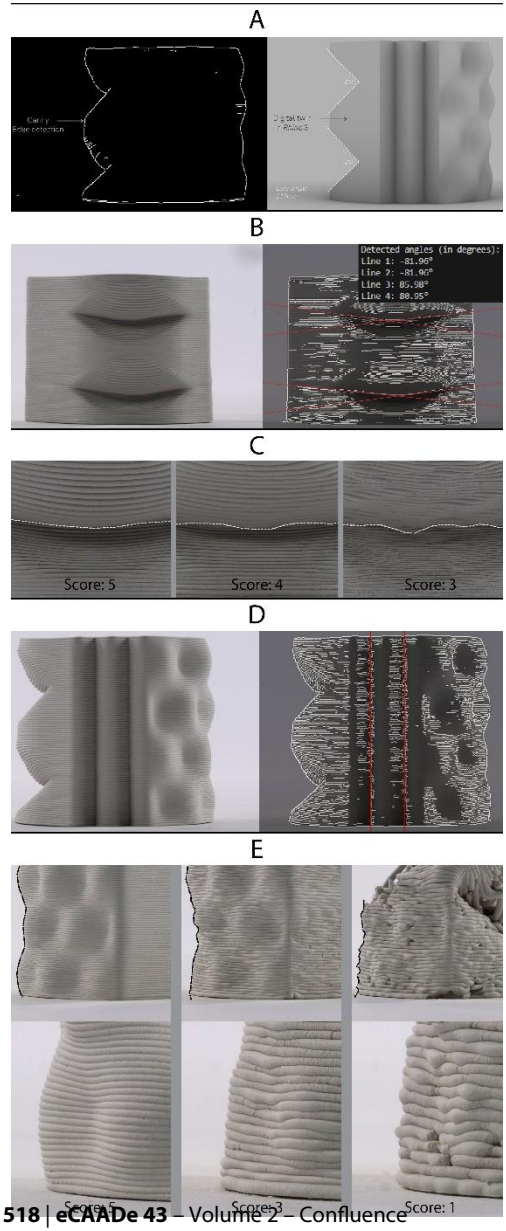

Figure 2
The methods for rating the specimens

The free-form pattern quality was rated by assessing the accuracy of concave-convex shapes and surface textures qualitatively (Figure 2-E).

The scores were compiled in a spreadsheet, resulting in an overall score for each specimen. They were used to determine whether a specimen should be considered good or bad while training the model.

Data preparation and labelling

The dataset created during specimen printing consists of 15,416 high-resolution images (4608 × 2592 pixels), which were captured every 3 seconds throughout the printing process. They were saved with corresponding metadata, including the G-code instance, timestamp, and file path. Figure 3 shows a sample of the photos taken during specimen printing. They are saved with a CSV file containing the metadata file path of the saved photos, timestamp, and fetched G-code instance.

Before labeling, the dataset was cleaned and organized by filtering out irrelevant data, adjusting the images, and updating the metadata. A Python script was used to remove a series of entries at the beginning and end of each specimen set to filter out irrelevant data. These were images and metadata collected before the actual printing began and after it had finished. For each specimen, 7 to 10 entries were removed using this method.

A separate Python script was used to adjust the images. The recorded image set was cropped around the identified nozzle center point and their resolution was reduced to 1280 × 720 pixels. A brightness adjustment was applied based on each specimen's external lighting conditions. Furthermore, the images were renamed according to each specimen's identity for easier referencing. Another Python script utilizing the pandas library and the regex pattern was used to update the metadata in a CSV file. The updated metadata included the standardized image path, time stamp, nozzle tip coordinates, and the relevant G-code parameters (LH: Layer Height and E: Extrusion Amount).

Figure 3
A sample of the recorded photos

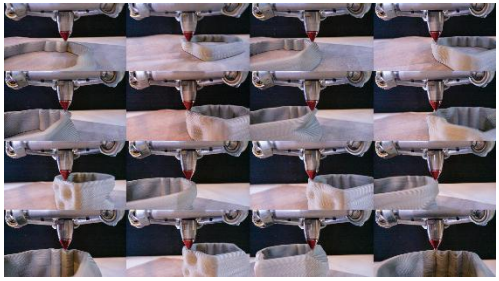

Figure 4
Data labeling matrix

To label the dataset, we used three categories: 0 (LOW), 1 (GOOD), and 2 (HIGH) for each parameter (Layer Height (LH) and Extrusion Amount (E)) similar to those presented by Brion and Pattinson (2022a, 2022b). Each image in the dataset received an output label corresponding to these categories. Based on the specimen ratings described in Section 2.4, we selected two 'standard' parameter combinations as references: (LH: 0.9 / E: 0.2) and (LH: 0.6 / E: 0.2), which represent the best-performing specimens. Using two standards instead of only one gave the model greater flexibility in learning the good printing parameters. All images from specimens with these combinations were labeled as (1,1), indicating both “Good LH” and “Good E”.

The complete dataset was labeled using a straightforward logic, as shown in Figure 4. Each dot on this graph represents a specimen characterized by a specific combination of parameters, with LH plotted on the vertical axis and E on the horizontal axis. The color of each dot indicates its assigned label (e.g., 2,2; 1,0; 1,1; 1,2; not printed). The gray dots indicate the label combinations that were not printed. The size of the dots represents how high the parameter values are in the whole model space. The arrows illustrate the calibration process used to reach the (1,1) label, which signifies “Good LH” and “Good E.

The labeling process included two steps. First, the Layer Height (LH) is assigned based on the closest "standard." Next, the Extrusion Rate (E) is assigned according to the closest "standard" while considering the previously assigned LH label. This method aimed to eliminate ambiguity arising from multiple standard values and provides a structured approach for dataset creation. For example, for the "LH: 0.9 / E: 0.8" combination, the closest "standard" value is "LH: 0.9 / E: 0.2". Thus, it first assigns an "LH: 1 (Good)" label as they are the same (0.9). Then, it assigns an "E: 2 (High)" label as 0.8 is higher than 0.2. Therefore, this combination is assigned with an "LH: 1 / E: 2" label.

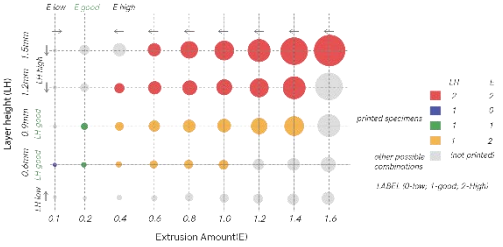

Machine learning method

We used the Attention-56 network developed by Wang et al., (2017) within a multi-head architecture, similar to its application for defect detection in Brion and Pattinson (2022a, 2022b) for classifying image-based quality parameters in Fused Deposition Modeling (FDM) plastic printing. Our approach adapts this machine learning process for clay printing by adjusting essential parameters such as layer height and extrusion amount.

The model has a shared backbone composed of residual and attention modules that enhance its robustness against noisy labels. Its multi-head design allows multi-label classification by extracting visual features and predicting relevant printing parameters, identifying good or poor printing quality characteristics. The backbone includes three attention modules to help the model focus on important image details and six residual blocks to improve learning efficiency by smoothly allowing information to skip over complex layers.

The attention masks created by this method help the model focus on the most important parts of an image. Hence, it can recognize subtle and

complex details more effectively. For example, an original input image (1280 x 720 pixels) is resized and augmented (adjusted through rotation, scaling, mirroring, brightness changes, and normalization) to teach the model to recognize features under different conditions. This modified image then passes through three separate attention mask modules, each trained to highlight specific key areas of the image while ignoring less important regions. Each module creates 256 mask channels.

These attention masks are placed on top of the original image at each step to show how each module works. Module 1 highlights the general printing area, module 2 focuses on the tip of the nozzle, and module 3 emphasizes the nozzle's edge. Reviewing all mask channels from each module provides a broader understanding of the patterns each module tends to focus on. This visualization approach shows what the neural network is paying attention to at each stage. It demonstrates how attention masks help the model pinpoint important areas for better detection and understanding.

Training the machine learning model

The training process for our model was conducted systematically over several rounds. Each round addressed specific challenges identified during the early stages and reflected on experiences from previous rounds.

The initial training rounds did not consistently produce accurate predictions, likely due to the limited number of samples labeled as (1,1). To address this issue, we printed additional specimens to increase the quantity of (1,1) data. Our goal was to help the model learn the characteristics of optimal printing parameters more effectively. However, problems with prediction accuracy continued, which we attribute to the overall imbalance in the dataset.

In the following rounds, we applied Class Balancing Techniques (CBT) to address the imbalanced distribution of categories within the dataset. We implemented CBT through upsampling, downsampling, and adjusting class weights to create a more balanced distribution. These changes improved the model's predictive performance, as reflected in the confusion matrices. In other words, the model made correct predictions more consistently across all categories.

In the final round, we utilized the imbalanced dataset of 15,416 images. We applied two CBT strategies to address the class imbalance: upsampling and downsampling (Model 6.0) and class weighting (Model 6.1). These balancing techniques aligned the validation loss curve more closely with the training loss curve, as shown in Figure 5. The figure shows the training and validation loss curves (left) and confusion matrices for Model 6.0. This indicates an improvement in the model's generalization across all classes. Compared to the earlier models, which used the imbalanced dataset without any balancing techniques, both methods significantly enhanced the model's generalizability.

As seen in the figure, the training and validation curves converge, which indicates a well-trained model. The heat maps on the right indicate the probability of predicted and True labels for both parameters (LH and E). Yellow indicates a higher probability of predicted labels. Model 6.0 achieved more balanced predictions across all classes, suggesting that upsampling and downsampling are more effective at handling class imbalance in large datasets than using class weights. Therefore, we selected Model 6.0, with upsampling and downsampling, as the final model for the calibration process.

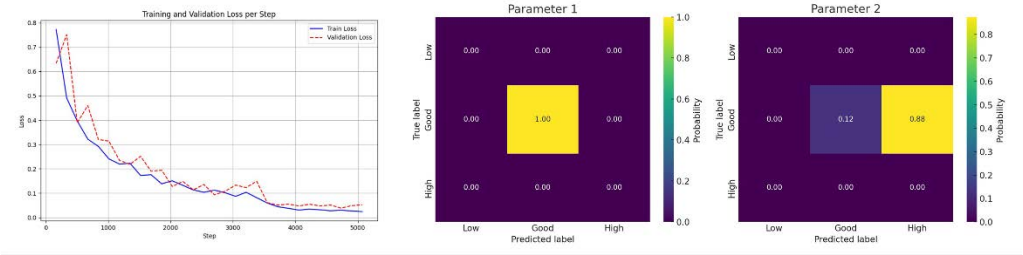

Figure 5
Training and validation loss curves and confusion matrices for Model 6.0

Automated adjustment of printing parameters

We aimed to develop an automated workflow to help the system identify optimal printing parameters (layer height and extrusion amount) through a calibration test before printing the final object (Figure 6). It was developed in Python to initiate the calibration process, capture real-time images to predict quality labels, adjust the printing parameters until satisfactory results are achieved, and then start printing the final object by updating the G-code with the predicted optimal parameters.

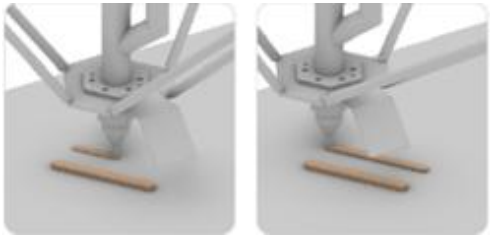

Figure 6
Calibration test design

The calibration test is an iterative closed-loop process that begins by printing a straight line using the standard initial parameters (layer height and extrusion amount). The printed result is then captured through real-time imaging and analyzed by the machine learning model to predict more optimal parameters based on learned visual features.

Subsequently, another calibration line is printed with these automatically adjusted parameters. This cycle repeats iteratively, and the model continuously refines its predictions until a satisfactory print quality is achieved, as confirmed by the predictive labels and confusion matrix analysis.

RESULTS

Figure 7 shows how the print quality improved in the calibration tests and reached an optimal result in six steps from left to right. The first line was printed with a 1.2 mm layer height and a 0.6 extrusion amount. In the last line, the layer height was set to 0.6, and the extrusion amount was set to 0.1. We evaluated this as a better print that performed smoother texture and a more uniform shell thickness on all layers.

Even though the calibration tool did not consistently achieve (1,1), it improved printing quality. Eventually, a complex-shaped object was printed using the most optimal parameters predicted by the ML model (LH: 0.6 / E: 0.1). This served as a preliminary validation to assess whether these selected parameters could successfully print intricate designs. The test object was designed as a clay wall tile with detailed geometric patterns, measuring 145 mm in width and 245 mm in height (Figure 8). The result was successful, indicating promising outcomes for future projects.

Figure 7
Calibration test results

CONCLUSIONS

The system presented in this paper is a work in progress. It shows how ML and computer vision can enhance the quality of 3DCP and make it possible to produce complex shapes with less human intervention needed to adjust the printing parameters. It provides useful results and indicates directions for future research.

Figure 8
The clay wall tile

The calibration test noticeably improved print quality through automated adjustments of layer height and extrusion amount. However, the system did not consistently achieve the desired (1,1) label. Further research is needed to understand the cause of this and its implications for the final print performance. The dataset generalization and model deployment strategies can be improved in future research.

We found that Class Balancing Techniques (CBT) are crucial for model performance. A balanced dataset usually gives the best results. When perfect balance is not achievable, upsampling and downsampling techniques are more effective than just class weighting. Training on an imbalanced dataset without adjustments lowers accuracy, particularly for minority classes. Thus, class imbalance must be addressed to enhance model generalization and fairness.

Data should be collected in consistent lighting to ensure accurate results. This consistency should also be kept during production. Including diverse lighting conditions can also help the model adapt to different real-world situations.

The camera was fixed next to the extruder to capture images from a steady angle. This works for simple geometries but is limiting for complex shapes. A 6-axis robot arm could let the camera rotate with the extruder and maintain a consistent angle to the nozzle. It could also integrate a light source targeting the nozzle for more consistent lighting along the toolpath.

One challenge during data collection was the mismatch between captured images and their corresponding G-code instances. The G-code often lagged behind the nozzle position due to system delays. While this didn't affect the current phase, it could limit future training tasks that need precise image-parameter correlations. Thus, we avoided capturing images more frequently than every three seconds. Simultaneous G-code recording and image capture caused lag in our Raspberry Pi-based system. An improved code or more efficient data transfer between the WASP printer and Raspberry Pi could resolve this issue and allow for more frequent image captures and better dataset reliability.

We assumed the clay mixture to be stable, but in practice, it was not. Measurements before loading into the tank showed varying water content. This can cause viscosity changes even during a single print. The viscosity also changes over time in the tank. It can affect material flow and print quality. Closed-loop systems that allow real-time monitoring and adjustment can be addressed in future research to solve this issue.

This work is applied to small-scale samples, focusing on geometrical and visual features. Factors like structural integrity and layer bonding are also crucial for architectural applications. Print speed also plays a significant role due to the large size of printed elements. So, visual feature assessment must be expanded to address these challenges and integrated with relevant process parameters in future research. Additionally, controlling other printing parameters, like speed, could be possible by increasing the number of heads in the ML framework and the dataset.

The model was trained on complex geometries, while the calibration relies on straight lines. This can impact the method's robustness. Its sensitivity to different geometries must be addressed in future research. While in our work it performed well on unseen images with familiar shapes, its performance declined when faced with new, unfamiliar geometries, such as the calibration line . This limitation indicates a need for more diversity in the dataset to enhance the model's adaptability. Alternatively, it may be necessary to limit its application to geometries that closely align with the training data.

ACKNOLWEDGEMENTS

The authors acknowledge the support of Paul de Ruiter, Vera Laszlo, and Henry Kiksen during the printing experiments at LAMA (Laboratory of Additive Manufacturing in Architecture), and Prateek Bhustali during ML model training.

REFERENCES

Akhavan, J., Lyu, J. and Manoochehri, S. (2024). 'A deep learning solution for real-time quality assessment and control in additive manufacturing using point cloud data' *Journal of Intelligent Manufacturing,* 35, pp. 1389-1406. Available at: https://doi.org/10.1007/s10845-023-02121-4.

Alqenaee, A. Y., Memari, A. M. and Hojati, M. (2021) 'Transition from traditional cob construction to 3D Printing of clay homes', *Journal of Green Building,* 16, pp. 3-28. Available at: https://doi.org/10.3992/jgb.16.4.3.

Asaf, O., Bentur, A., Larianovsky, P. and Sprecher, A. (2023). 'From soil to printed structures: A systematic approach to designing clay-based materials for 3D printing in construction and architecture', *Construction and Building Materials,* 408. Available at: https://doi.org/10.3992/jgb.16.4.3.

Bhandarkar, V. V., Kumar, A. and Tandon, P. (2025). Warpage detection in 3D printing of polymer parts: a deep learning approach. *Journal of Intelligent Manufacturing,* 36, pp. 3129–3141. Available at: https://doi.org/10.1007/s10845-024-02414-2.

Brion, D. A. J. and Pattinson, S. W. (2022a) 'Quantitative and real-time control of 3D printing material flow through deep learning', *Advanced Intelligent Systems,* 4(11). Available at: https://doi.org/10.1002/aisy.202200153.

Brion, D. A. J. and Pattinson, S. W. (2022b) 'Generalisable 3D printing error detection and correction via multi-head neural networks', *Nature Communications,* 13. Available at: https://doi.org/10.1038/s41467-022-31985-y.

Chan, S. S. L., Pennings, R.M., Edwards, L. and Franks, G. V. (2020) '3D printing of clay for decorative architectural applications: Effect of solids volume fraction on rheology and printability', *Additive Manufacturing,* 35. Available at: https://doi.org/10.1016/j.addma.2020.101335.

Curth, A., Pearl, N., Castro-Salazar, A., Mueller, C. and Sass, L. (2024) '3D printing earth: Local, circular material processing, fabrication methods, and life cycle assessment', *Construction and Building Materials,* 421. Available at: https://doi.org/10.1016/j.conbuildmat.2024.135714.

Davtalab, O., Kazemian, A., Yuan, X. and Khoshnevis, B. (2020) 'Automated inspection in robotic additive manufacturing using deep learning for layer deformation detection', *Journal of Intelligent Manufacturing,* 33, pp. 771-784.

Available at: https://doi.org/10.1007/s10845-020-01684-w.
El Aabbas, M., Mahdaoui, M., Ahachad, M., Mazian, B., Aalil, I. and Ouardouz, M. (2024) 'Advancing sustainable construction: Terracotta component development through extrusion-based 3D printing with local clay', *Construction and Building Materials,* 442. Available at: https://doi.org/10.1016/j.conbuildmat.2024.137549.
Farrokhsiar, P., Gursoy, B. and Duarte, J. P. (2024) 'A comprehensive review on integrating vision-based sensing in extrusion-based 3D printing processes: toward geometric monitoring of extrusion-based 3D concrete printing', *Construction Robotics,* 8. Available at: https://doi.org/10.1007/s41693-024-00133-x.
Geng, S., Luo, Q., Liu, K., Li, Y., Hou, Y. and Long, W. (2023) 'Research status and prospect of machine learning in construction 3D printing', *Case Studies in Construction Materials,* 18. Available at: https://doi.org/10.1016/j.cscm.2023.e01952.
Gomaa, M., Jabi, W., Soebarto, V. and Xie, Y. M. (2022) 'Digital manufacturing for earth construction: A critical review', *Journal of Cleaner Production,* 338. Available at: https://doi.org/10.1016/j.jclepro.2022.130630.
Gomaa, M., Jabi, W., Veliz Reyes, A. and Soebarto, V. (2021) '3D printing system for earth-based construction: Case study of cob', *Automation in Construction,* 124. Available at: https://doi.org/10.1016/j.autcon.2021.10357/.
Gündüz, G. and Özkar, M. (2024) 'A process-based framework for adaptable modules in robotic clay 3D printing', *International Journal of Architectural Computing,* 22(1). pp. 45-61. Available at: https://doi.org/10.1177/14780771231225698.
Jauk, J. (2025). *Termite*. Available at: https://www.food4rhino.com/en/app/termite
Kazemian, A., Yuan, X., Davtalab, O. and Khoshnevis, B. (2019) 'Computer vision for real-time extrusion quality monitoring and control in robotic construction', *Automation in Construction,* 101, pp. 92-98. Available at: Available at: https://doi.org/10.1016/j.autcon.2019.01.022.
Keep, J. (2020) *Formulating and testing a clay body for extrusion clay 3D printing* [Online]. Available at: http://www.keep-art.co.uk/Journal/Test_FormulatingClayBody.pdf
Keramikos. (no date). *3D Prai* [Online]. Available at: https://www.keramikos.nl/3d-klei/15347-3D-Prai.html (Accessed 31 March 2025)
OctoPrint. (no date). *OctoPrint* [Online]. Available at: https://octoprint.org/ (Accessed 31.03.2025)
Perrot, A., Rangeard, D. and Courteille, E. (2018) '3D printing of earth-based materials: Processing aspects', *Construction and Building Materials,* 172, pp. 670-676. Available at: https://doi.org/10.1016/j.conbuildmat.2018.04.017.
Singh, M., Sharma, P., Sharma, S. K. and Singh, J. (2025) 'A novel real-time quality control system for 3D printing: A deep learning approach using data efficient image transformers', *Expert Systems with Applications,* 273. Available at: https://doi.org/10.1016/j.eswa.2025.126863.
Taher, A., Aşut, S. and van der Spoel, W. (2023) 'An integrated workflow for designing and fabricating multi-functional building components through additive manufacturing with clay', *Buildings,* 13(11). Available at: https://doi.org/10.3390/buildings13112676.
Wang, F., Jiang, M., Qian, C., Yang, S., Li, C., Zhang, H., Wang, X. and Tang, X. (2017) 'Residual attention network for image classification', *Proceedings of the IEEE conference on computer vision and pattern recognition*. pp. 3156-3164. Available at: https://doi.org/10.48550/arXiv.1704.06904.
Wang, W., Wang, P., Zhang, H., Chen, X., Wang, G., Lu, Y., Chen, M., Liu, H. and Li, J. (2024) 'A real-time defect detection strategy for additive manufacturing processes based on deep learning and machine vision technologies', *Micromachines,* 15(1). Available at: https://doi.org/10.3390/mi15010028.